

Predicting wheat kernels' protein content by near infrared hyperspectral imaging

Yang Shuqin¹, He Dongjian^{1*}, Ning Jifeng²

(1. College of Mechanical and Electronic Engineering, Northwest A&F University, Yangling 712100, China;

2. College of Information Engineering, Northwest A&F University, Yangling 712100, China)

Abstract: The objective of this study was to explore the potential of near infrared hyperspectral imaging combined with statistical regression models and neural networks for nondestructive prediction of protein content of wheat kernels. Seventy-nine samples from 11 breeds of wheat kernels were collected. The protein percentage of each sample measured by semimicro-Kjeldahl method was taken as the reference value. After comparing the prediction models of principal components regression (PCR) and partial least squares regression (PLSR) with various pretreatment methods, PLSR preprocessed by zero mean normalization (z score) function of MATLAB was found to obtain better prediction results than other regression models. Based on 10 latent variables of PLSR, the radial basis function (RBF) neural network was applied to improve the prediction, in which the coefficients of determination (R^2) were greater than 0.92 for both the calibration set and validation set, while the corresponding *RMSE* values were 0.3496 and 0.4005, respectively. Therefore, hyperspectral imaging can provide a fast and non-destructive method for predicting the wheat kernels' protein content.

Keywords: wheat kernels, protein, nondestructive prediction, near infrared hyperspectral imaging, partial least squares regression, radial basis function neural network

DOI: 10.3965/j.ijabe.20160902.1701

Citation: Yang S Q, He D J, Ning J F. Predicting wheat kernels' protein content by near infrared hyperspectral imaging. Int J Agric & Biol Eng, 2016; 9(2): 163–170.

1 Introduction

As a cereal crop with high protein, wheat is one of the main sources of protein for human food and livestock feed, whose protein content accounts for 10%-18% of total kernel's weight. The quantity and quality of protein largely determine the nutrition value and the taste of the wheat products, such as noodles, bread, pasta, and so on. That is to say, protein is an important indicator of the wheaten food.

Several chemical and physical methods have been established and applied for detecting the protein content, such as Kjeldahl method^[1], Dumas (Nitrogen Combustion) method^[1,2], Biuret method^[3], Lowry method^[4], and Dye-Binding methods^[5]. Nevertheless, these methods are weak at timeliness with high cost and invasive to the food materials in most cases. With the development of image technology and machine vision, infrared spectroscopy, especially near infrared (NIR) reflection, could achieve rapid and non-invasive detection without chemical consumption and environment contamination, so many researchers tried to use this kind of chemical-free method to assess the attributes of food. Bogomolov et al.^[6] used light scatter of visible and adjacent near infrared region to measure the fat and total protein in milk. Kays et al.^[7] investigated the potential of near infrared spectroscopy for the analysis of protein in a data set that included food products with different kinds of cereals. Pohl et al.^[8] used the principal component analysis (PCA)

Received date: 2015-01-25 **Accepted date:** 2015-11-02

Biographies: Yang Shuqing, PhD, Associate Professor, Major in intelligent detection and monitoring, Email: yangshuqin1978@163.com; Ning Jifeng, PhD, Associate Professor, Major in machine vision, Email: jf_ning@sina.com.

***Corresponding author:** He Dongjian, PhD, Professor, Majoring in image analysis and recognition, agricultural information technology, and intelligent detecting and control. Mailing address: No.22 Xinong Road, Yangling, Shaanxi 712100, China, Tel: +86-29- 87092391; Email: hdj168@nwsuaf.edu.cn.

and the partial least squares regression (PLSR) to evaluate the cereal grains in bioethanol production after scanned by NIR system. Norgaard et al.^[9] took more than 40 000 wheat samples and designed an artificial neural network (ANN) to model the relationship between the protein and NIR value. However, a traditional infrared camera only covers a small region of the research object, which could generate inaccurate detecting results when some features are uneven inside the material.

As a prominent technology of analyzing biological and food samples, hyperspectral imaging has attracted more and more attention in recent years. Hyperspectral images contain two spatial dimensions and one spectral dimension with contiguous bands. Therefore, a hyperspectral image can be taken as a data cube $I(x, y, \lambda)$, in which $I(x, y)$ is the spatial position of a pixel, and $I(\lambda)$ stands for the wavelength. Unlike the previous spectroscopy, the information of each pixel in the hyperspectral image could cover a complete spectrum throughout the visible, near-infrared and/or short wave region. Because NIR has strong ability of penetration, the hyperspectral image could fully reflect a sample's external morphology characteristics and the internal distribution of diverse chemical compositions^[10-12]. Hyperspectral imaging (HSI) technology with combination of some pattern

recognition and machine learning methods is accepted as the most reliable and nondestructive analytical tool in detection of contaminations, identification of defects and quantification of constituents for guaranteeing food quality and safety. For example, according to Barbin et al.^[13] and Bhuvaneshwari et al.^[14], NIR reflection in HSI could determine the chemical composition in pork or detect insect fragments in semolina. Serranti et al.^[15] obtained the hyperspectral images of the oat and groat kernels in the NIR range (1006-1650 nm), and used only three wavelengths (1132 nm, 1195 nm and 1608 nm) to classify those kernels. Similarly, Choudhary et al.^[16] combined PCA on wavelet texture and infrared HSI to sort eight Western Canadian wheat classes in bulk samples.

The objective of this study was to investigate the feasibility of NIR hyperspectral imaging combined with the regression models of principal component regression (PCR) and PLSR and neural networks of the radial basis function (RBF) to predict protein content of wheat kernels.

2 Materials and methods

Figure 1 shows the main procedures of prediction of wheat's protein based on hyperspectral images in this study, which will be explained in the following sections in detail.

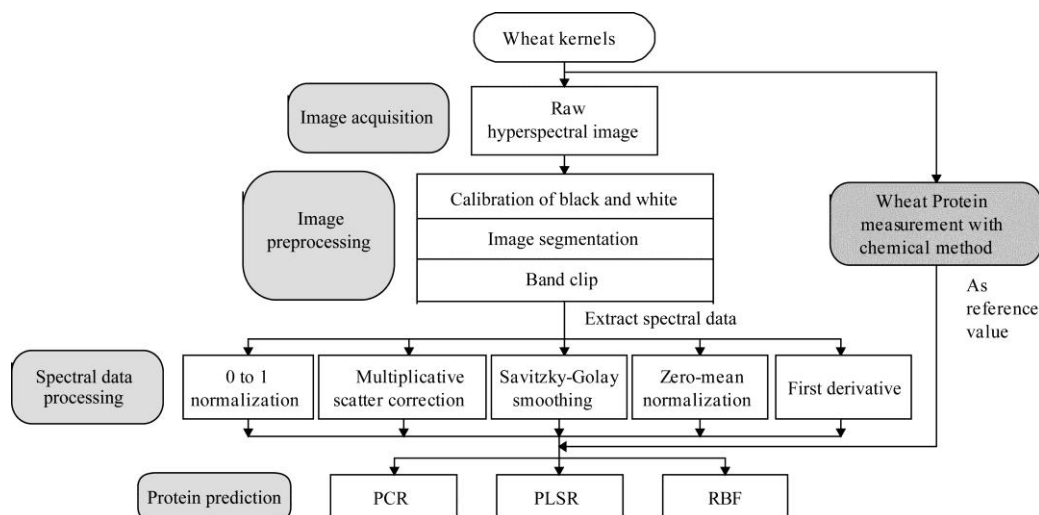


Figure 1 Flow chart of prediction of wheat kernels' protein content by hyperspectral images

2.1 Wheat kernels samples

Seventy-nine samples in this study were randomly collected from 11 breeds of wheat samples, including Abo (8), Gao9411 (7), Han6172 (7), N9659 (6), Wan33 (8), Wenmai6 (8), Xiaoyan No.6 (8), Xinong1376 (6),

Zhengnong16 (7), Zhongyu6 (8), and Zhou13 (6). Wheat kernels of these samples were grown in the wheat field of Northwest A&F University under the same cultivated conditions and harvested in June 2013. They were all kept in the environment with the normal temperature after

they dried sufficiently. Each sample contained 20 g of a single breed of wheat kernels. For each wheat breed, 4-6 samples were randomly selected to compose the calibration set, and the rest of the samples were used as the testing set for assessment of their protein contents.

2.2 NIR hyperspectral imaging system

NIR hyperspectral image acquiring system consists of a hyperspectral spectrograph (ImSpector N17E, Spectral Imaging Ltd., Finland), a CCD camera (XEVA2616, XenICs Ltd., Belgium), a dark box with a motorized translation stage and a lighting unit of four 100 W halogen lights. The spectrograph's spectral range is from 900 nm to 1700 nm, and the resolution is 2.8 nm. The CCD camera has 320×256 pixels. After adjusted by black and white correction, the HSI data can be acquired by this pushbroom system in line scanning mode.

2.3 Image acquisition

To avoid the baseline shift, the HSI system was turned on and preheated for 30 min. The hyperspectral images were acquired with the help of Spectral SECN-V17E software (Gilden Photonics Ltd., England) with the wavelength resolution of 3.32 nm, the exposure time of 10 ms and the stage speed of 20 mm/s. Hyperspectral image extraction was performed by the ENVI 4.7 (Research Systems Inc., Boulder, Co, USA).

Owing to the uneven distribution of illuminant and dark current of the camera, the hyperspectral image will have greater noise in the bands with weak light intensity. So the raw image, *I*, needs to be calibrated prior to image processing. Under the same condition with raw image acquisition, the white reference image, *W*, was captured with a white Teflon calibration tile, while the black reference image, *B*, was acquired after turning off the lighting source and closing camera's lens cap. Then, the raw images were transformed to the relative image, *R*, using Equation (1).

$$R = (I - B) / (W - B) \tag{1}$$

2.4 Spectra preprocessing

To explore the relationship between hyperspectral image of wheat kernels and protein content, spectra of ROI (region of interest) should be extracted from background. Besides, raw curves of the NIR spectrum still have some noise especially in lower wavelengths and higher

wavelengths. This unreliable information will disturb the subsequent analysis and need to be discarded in the image preprocessing. All image processing was completed using MATLAB (R2013b; Math Works, Inc., USA).

The hyperspectral image of one sample at 950 nm in Figure 2a, was taken as an example, in which the wheat kernels region is the ROI. Figure 2b shows the spectral profiles of one pixel of the wheat kernels and one pixel of the background with 256 bands (865-1711 nm) of this sample. It can be seen that there exists obvious difference between the reflection curve of wheat kernel and that of background. Therefore, the process of band ratio between 1084 nm and 1449 nm combined with morphological open and close operations were used to define a mask to remove the background in the image (see Figure 2). Then, the average spectrum of ROI in each sample was calculated.

In view of high noise in both ends of the NIR spectral region, the wavelength range was limited to 231 bands in the middle (928-1695 nm) by band clip. The spectral data of all samples could be extracted in the same way. The average spectra curves of 79 samples after band clip are shown in Figure 2d). These curves contain the main key spectral information of ROI.

2.5 Wheat protein measurement with chemical method

After acquiring the raw hyperspectral images of the wheat kernels, the semimicro-Kjeldahl method^[17] was used to get the protein contents of 79 samples as the reference value. In this method, the crude protein nutrition is determined by measuring the total organic nitrogen. For protein decomposition, the sample of wheat kernels is powdered and heated to digest with sulfuric acid and catalyst. The decomposition of ammonia and sulfuric acid combined into ammonium sulfate. Then the ammonia dissociated by alkalifying and distilling was absorbed by boric acid. The boric anions formed are titrated with standardized acid. Finally, the protein content is calculated by the product of the consumption of acid and the conversion factor (see Equation (2))^[17,18].

$$Pro\% = 2N_{H_2SO_4} \times \frac{V_1 - V_2}{W} \times 14 \times F \times 100 \tag{2}$$

where, *Pro%* is the percentage of protein; the number 2

stands for that one sulfuric acid react with two amino; $N_{H_2SO_4}$ is normality of H_2SO_4 , mol/L; V_1 is the volume of standard acid for wheat sample, mL; V_2 is the volume of standard acid for blank, mL; $V_1 - V_2$ is the corrected acid

volume; W is the weight of sample, in g; 14 is atomic weight of one mole nitrogen, in g; $F=5.70$, a factor for wheat of converting the percentage of nitrogen to the percentage of crude protein.

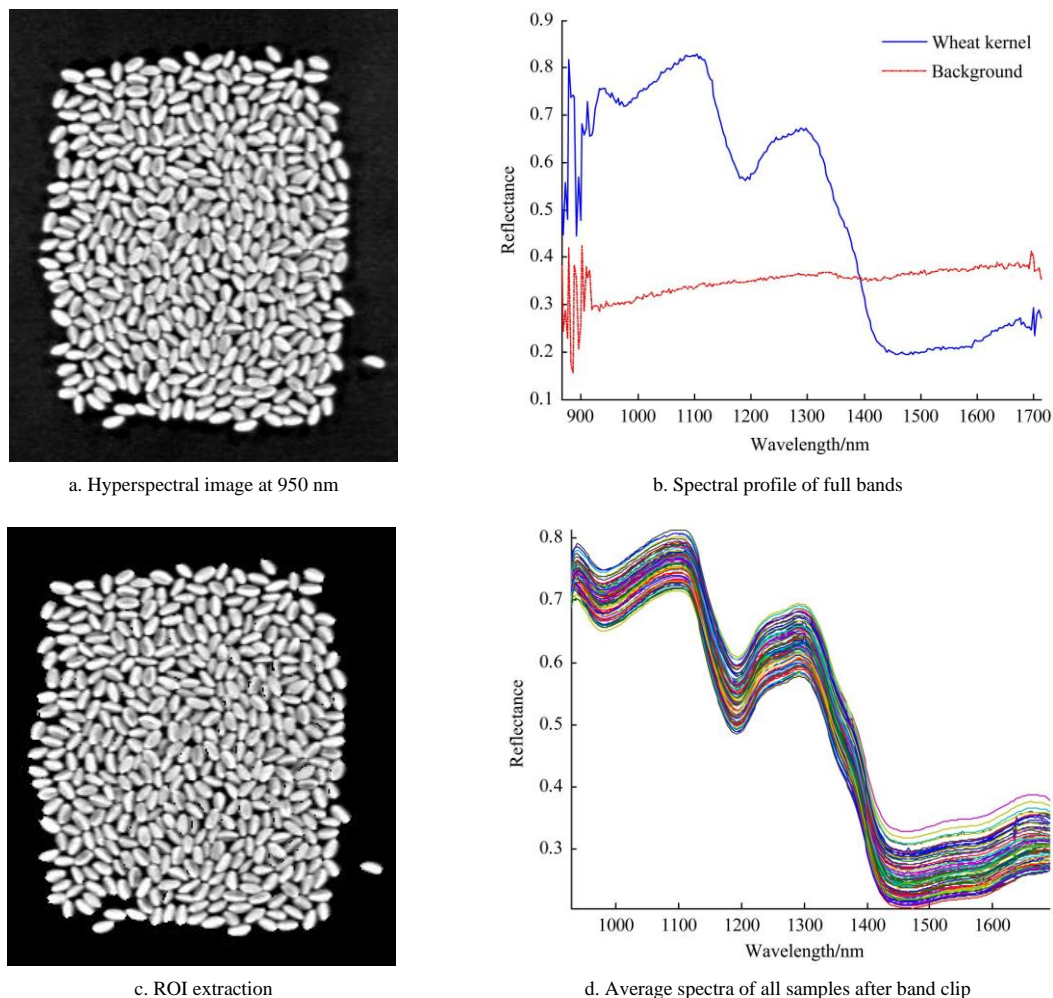


Figure 2 Extracting the spectral data of the region of interest (ROI)

2.6 Spectral data pretreatment

For modeling and verifying, 4-6 samples were randomly chosen for each wheat breed to form calibration samples, while the rest 22 samples were used for prediction. To reduce the influence of high-frequency random noises, the nonuniformity and the surface scattering of the wheat kernels, the spectral data were subjected to five commonly used chemometrics pre-treatments respectively: 0 to 1 normalization (01 normalization), multiplicative scatter correction (MSC), Savitzky-Golay (SG) smoothing, zero mean normalization (z score) and first derivative (1-Der). For these five pre-treatment methods, 01 normalization could unify the statistical distribution of samples; MSC reduces the influence the feature of surface scatter and the variance of

optical length on spectrum; SG smoothing could maintain the spectrum's profile by removing the temporal energy surge of noises; z score scales data set using the mean value and the standard deviation; and 1-Der is often used for removing the disturbance caused by background.

2.7 Building prediction models

One of the challenges in analyzing hyperspectral data is to solve the problem of multicollinearity in HSI data, i.e. redundancy. Redundant information in hyperspectral image will slow down the processing speed and accuracy. After band clipping, principal components regression (PCR) and partial least square regression (PLSR) were employed to reduce the redundancy and speed up the data analysis and processing. These two regression models could extract main spectrum information from voluminous data.

For PCR, the spectrum matrix needed to be centralized at first. Then, through estimating eigenvalue decomposition of the covariance matrix, those eigenvectors with large eigenvalues, so called principal components, were used to form the projection matrix. At last, the original spectrum matrix was projected to get a new sample matrix with low dimension. We decided the number of principal components in PCR by the percentage variance explained in spectral reflection.

For PLSR, the matrix of pretreated spectra data and the protein percentage vector measured by chemical method were specified as independent (X) and dependent (Y) respectively. X and Y were analyzed by principal component decomposition with non-linear iterative partial least squares (NIPALS). This decomposition process took the linear relationship between X and Y into account. After switching X and Y as iteration variable repeatedly, X was transferred into the matrix of latent variables. The number of best latent variables in PLSR was determined by 10-fold cross validation (CV). The smaller the components (principal components or latent variables) number, the lower the dimension of model was.

Based on the reduced data by PCR or PLSR, radial basis function (RBF) neural network will be applied to improve the forecasting. RBF network is a three-layer feedback network model, which includes input layer, hidden layer and output layer. The hidden layer uses RBF as the base of hidden unit. We took radial Gaussian function (Equation (3)) as activation function for hidden layer in this research. Equation (4) gives the output of the network. The input data of RBF network can be transformed from low dimensional space to high dimensional space so as to change each linearly inseparable problem into a separable one.

$$R(x_p - c_i) = \exp\left(-\frac{1}{2\sigma^2} \|x_p - c_i\|^2\right) \quad (3)$$

$$o_j = \sum_{i=1}^h w_{ij} \cdot R(x_p - c_i) \quad (4)$$

where, $R(x_p - c_i)$ is the activation function; $x_p = (x_1^p, x_2^p, \dots, x_m^p)$ is the p^{th} input sample; c_i is the center of the Gaussian function, $i=1,2,\dots,h$, while h is the number of hidden nodes. $\|x_p - c_i\|^2$ is their Euclidean distance; σ is the

variance of the Gaussian function; o_j is the actual output of the j^{th} output node; w_{ij} is the connection weight between the hidden layer and output layer, which is obtained by the least mean square algorithm.

To measure the model's performance and select the best model, several indicators in the calibration set and the validation set were adopted, such as the mean square error in 10-fold CV ($RMSECV$), coefficients of determination (R^2 , Equation (5)), the root mean square errors ($RMSE$, see Equation (6)) and the relative percentage difference ($RPD\%$, Equation (7)). MSE in 10-fold CV, R^2 and $RMSE$ in the calibration set could evaluate the model's robustness, while R^2 , $RMSE$ and $RPD\%$ in validation set is for assessment of prediction.

$$R^2 = 1 - \frac{\sum_i (y_i - f_i)^2}{\sum_i (y_i - \bar{y})^2} \quad (5)$$

$$RMSE = \sqrt{\frac{1}{n-1} \sum_i (y_i - f_i)^2} \quad (6)$$

$$RPD\% = \text{mean}\left(\frac{\text{abs}(f_i - y_i)}{(f_i + y_i) / 2}\right) \quad (7)$$

where, f_i is the predict protein content percentage of the i^{th} sample by prediction model; y_i is the reference protein content percentage of the i^{th} sample obtained by the chemical method; n is the number of samples; \bar{y} is the mean protein content percentage of the sample set.

All the prediction models were developed with MATLAB R2013b.

3 Results and discussion

3.1 Partition of sample set

Table 1 presents the descriptive statistics such as the range, mean, and standard deviation (STD) of samples' protein content acquired by semimicro-Kjeldahl method. As shown in Figure 3, the range of protein content varies with wheat breed, and the protein content percentage of each breed is concentrated around its mean value with relatively small vibration, in which the tick labels of x axis stand for sample index, for example, 1-8 are Abo, 9-15 are Gao9411, 16-22 are Han 6172, etc. In the last three rows of Table 1, the statistics for the whole set, calibration set and validation set are listed.

Table 1 Simple statistics of protein content for different wheat breeds and partition sets

Sample	Number of samples	Protein range/%	Mean/%	STD
Abo	8	14.21-14.87	14.4438	0.2609
Gao9411	7	12.48-12.76	12.6543	0.0938
Han6172	7	11.88-12.84	12.4314	0.2907
N9659	6	15.49-17.07	16.4200	0.6133
Wan33	8	11.88-12.75	12.3025	0.3086
Wenmai6	8	12.80-13.20	12.9763	0.1739
Xiaoyan No.6	8	14.41-14.77	14.5975	0.1427
Xinong1376	6	11.59-12.67	12.4233	0.4796
Zhengnong16	7	12.93-15.06	13.9200	0.6871
Zhongyu6	8	11.13-12.48	11.8588	0.3842
Zhou13	6	13.01-14.31	13.4150	0.4648
Whole Set	79	11.13-17.10	13.3673	1.3059
Calibration Set	57	11.13-17.07	13.3456	1.2793
Validation set	22	11.59-17.10	13.4236	1.4017

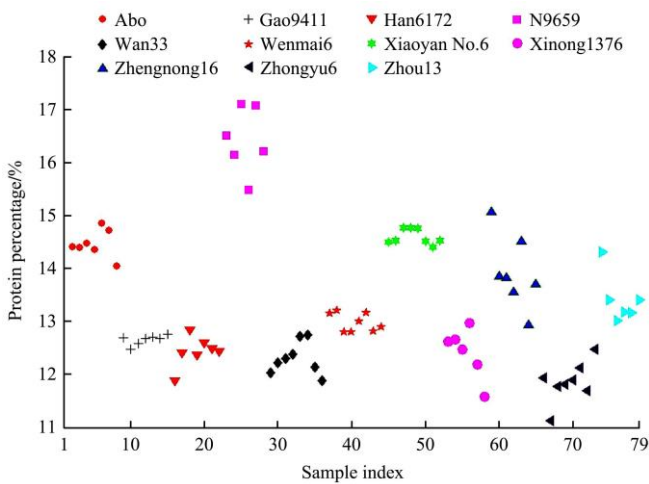


Figure 3 Distribution of protein content

3.2 Prediction methods

The data model with accurate prediction was expected to have fewer latent variables, greater R^2 and smaller $RMSE$ and $RPD\%$. Furthermore, the difference of indicators' value between the calibration set and the validation set should be as small as possible.

3.2.1 PCR

In the PCR model, the energy of the data concentrates on the first few principal components which usually reflect the data features with large correlation, while other components are about uncorrelated noise. Because the more energy the principal component has, the greater percentage it accounts for the variance explained in the spectrum, the original spectrum can be reconstructed by a few principal components.

For fitting the data, about twenty components can usually meet the need, but diagnostics from this fit can be

used to make a choice of a simpler model with fewer components. Figure 4 shows the cumulative percentage of variance of different pretreatment methods, in which each color zone corresponds to the explanation percentage of one principal component. It can be seen that the proportion of the first two principal components in the spectrum is great than 90% under most circumstances. However, in view of the fact that too few components will lead to large error in data approximation, the components number of PCR was determined when their total percentage exceeds 99.99% in this study.

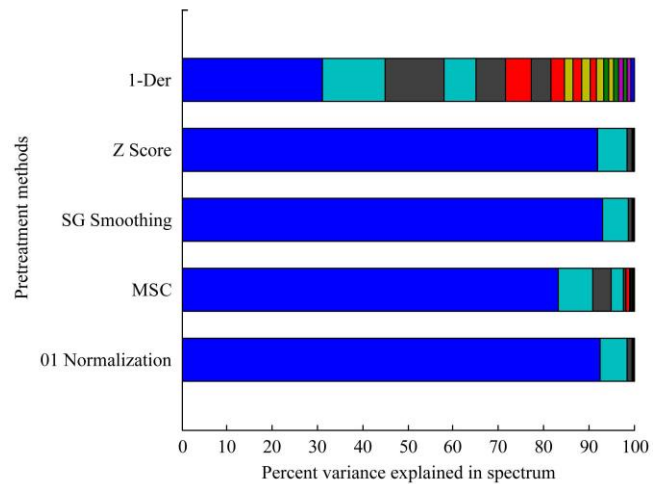


Figure 4 Energy percentage varying with the number of principal components in different pretreatments

Table 2 illustrates the results of PCR. It can be seen that, 1-Der used the most principal components (20), but achieved the smallest R^2 (0.5775 and 0.1050) and the largest $RMSE$ (0.8316 and 1.4735) and $RPD\%$ (8.4711), which suggest that 1-Der in PCR model is not suitable for preprocessing the hyperspectral data of wheat kernels. For the other methods, MSC performed best whether in the calibration set or in the validation set with largest R^2 (0.8137 and 0.8122) and smallest $RMSE$ (0.5522 and 0.6075) and $RPD\%$ (3.2965) at the expense of more principal components (19).

Table 2 Statistical indicators of different pretreatments in PCR

Pretreatment method	Principal components	Calibration set		Validation set		
		R^2	$RMSE$	R^2	$RMSE$	$RPD\%$
01 Normalization	10	0.6351	0.7728	0.7701	0.6721	3.9269
MSC	19	0.8137	0.5522	0.8122	0.6075	3.2965
SG Smoothing	8	0.6026	0.8065	0.7687	0.6742	3.8864
Z Score	10	0.6381	0.7696	0.7719	0.6695	3.9193
1-Der	20	0.5775	0.8316	0.1050	1.4735	8.4711

3.2.2 PLSR

As for the PLSR model, shown in Table 3, 1-Der method had the biggest R^2 (0.8843) and smallest $RMSE$ (0.4353) in the calibration set while the smallest R^2 (0.6885) and biggest $RMSE$ (0.7823) in the validation set, which proved the 1-Der method magnified the noise and caused overfitting for the wheat spectrum. Except for the 1-Der, there were no large differences in the indicators among the other pretreatment methods between the calibration set and the validation set. For the validation set, z score method corresponded to the greatest R^2

(0.8521) and the smallest $RMSE$ (0.5391), which means it has stronger generalization ability.

In general, PLSR performs better than PCR in prediction of wheat protein with fewer variables, higher R^2 and less $RMSE$ for both the calibration set and the validation set. Owing to its good performance in prediction, the dimension reduction spectra of the 10 latent variables selected by z score for PLSR were combined with RBF neural network to achieve a better prediction result.

Table 3 Statistical indicators of different pretreatments in PLSR

Pretreatment Method	Latent Variables	RMSECV	Calibration Set		Validation set		
			R^2	$RMSE$	R^2	$RMSE$	$RPD\%$
01 Normalization	9	0.6684	0.8390	0.5133	0.8413	0.5583	3.2678
MSC	9	0.6724	0.8557	0.4860	0.8264	0.5840	3.1208
SG Smoothing	11	0.7226	0.8561	0.4853	0.8401	0.5604	3.2636
Z Score	10	0.7214	0.8559	0.4857	0.8521	0.5391	3.1276
1-Der	10	1.1027	0.8843	0.4353	0.6885	0.7823	4.1331

3.2.3 RBF neural network

A RBF neural network was designed based on the 10 latent variables obtained in PLSR with z score. The mean squared error (MSE) goal and the spread speed of RBF are the only parameters needed to be fixed, which could be determined by cross validation. Figure 5 is the prediction result under the circumstance that MSE 's goal and RBF's spread speed are 0.12 and 0.6, respectively. The axes of X and Y represent the protein percent measured by chemical method and the protein percent predicted with RBF.

Figure 5 indicated that most fitting points are close to the 45° line. R^2 in both the calibration set and the validation set were greater than 92%, and $RMSE$ (0.3496 and 0.4005) went down to relatively small values, which proved that RBF network improved the prediction result apparently.

4 Conclusions

In this work, a pushbroom hyperspectral imaging system in the NIR region of 975-1522 nm was developed to evaluate the protein content percentage of wheat kernels from 11 breeds. Compared with other pretreatment methods in PCR and PLSR, PLSR with the pretreatment with z score had relatively better dimension-reduced spectrum data, whose 10 latent variables could achieve the R^2 of 0.8521, $RMSE$ of 0.5391 and $RPD\%$ of 3.1276. Furthermore, based on these data, RBF neural networks were employed to improve the forecasting of protein content. The results shows that RBF can fit both the calibration set and the validation set accurately with R^2 greater than 0.92 and $RMSE$ less than 0.41. This study suggests that hyperspectral imaging is promising for evaluating protein content of wheat kernels.

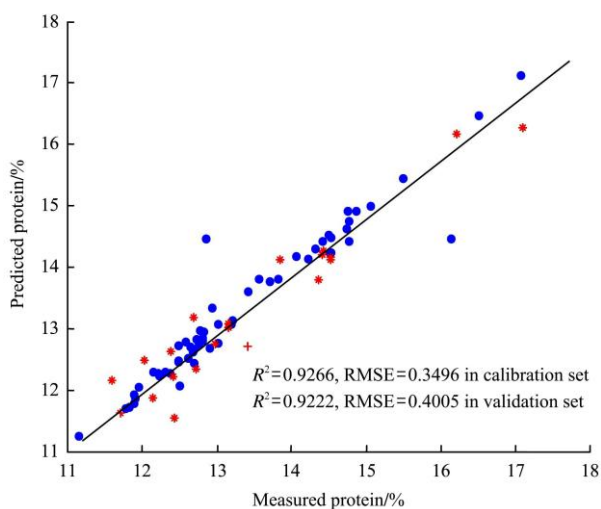


Figure 5 Prediction Result of RBF neural network

Acknowledgements

This study was funded by National Natural Science Foundation of China (31501228, 61473235, 41301450), Natural Science Foundation of Shaanxi Province (2015JM3110), Fundamental Research Funds for the Central Universities (Z109021561, QN2013062, 2452015381), Scientific Research Foundation for Doctor, Northwest A&F University (2012BSJJ027), Comprehensive Innovation Technology Project of Shaanxi Province (2015KTZDNY01-06) and Special Talent Fund of Shaanxi Province (Z111021303).

[References]

- [1] Jung S, Rickert D A, Deak N A, Aldin E D, Recknor J, Johnson L A, Murphy P A. Comparison of Kjeldahl and Dumas methods for determining protein contents of soybean products. *Journal of the American Oil Chemists' Society*, 2003; 80(12): 1169–1173.
- [2] Serrano S, Rincón F, García-Olmo J. Cereal protein analysis via Dumas method: Standardization of a micro-method using the EuroVector Elemental Analyser. *Journal of Cereal Science*, 2013; 58(1): 31–36.
- [3] Itzhaki R F, Gill D M. A micro-biuret method for estimating proteins. *Analytical Biochemistry*, 1964; 9(4): 401–410.
- [4] Markwell M A K, Haas S M, Bieber L L, Tolbert N. A modification of the Lowry procedure to simplify protein determination in membrane and lipoprotein samples. *Analytical Biochemistry*, 1978; 87(1): 206–210.
- [5] Bradford M M. A rapid and sensitive method for the quantitation of microgram quantities of protein utilizing the principle of protein-dye binding. *Analytical Biochemistry*, 1976; 72(1): 248–254.
- [6] Bogomolov A, Dietrich S, Boldrini B, Kessler R W. Quantitative determination of fat and total protein in milk based on visible light scatter. *Food Chemistry*, 2012; 134(1): 412–418.
- [7] Kays S E, Barton I I, Franklin E, Windham W R. Predicting protein content by near infrared reflectance spectroscopy in diverse cereal food products. *Journal of Near Infrared Spectroscopy*, 2000; 8(1): 35–43.
- [8] Pohl F, Senn T. A rapid and sensitive method for the evaluation of cereal grains in bioethanol production using near infrared reflectance spectroscopy. *Bioresource Technology*, 2011; 102(3): 2834–2841.
- [9] Norgaard L, Lagerholm M, Westerhaus M. Artificial Neural Networks and Near Infrared Spectroscopy-A case study on protein content in whole wheat grain. *Foss White Paper*. Available from: <http://www.foss.dk/campaign/-/media/242657904D734CE9B0652C3D885776AE.ashx>. Accessed on [2014-12-30]
- [10] Sun D W. *Hyperspectral imaging for food quality analysis and control*. Elsevier, USA, 2010.
- [11] Huang H, Liu L, Ngadi M O. Recent developments in hyperspectral imaging for assessment of food quality and safety. *Sensors*, 2014; 14(4): 7248–7276.
- [12] Wu D, Sun D W. Advanced applications of hyperspectral imaging technology for food quality and safety analysis and assessment: A review—Part I: Fundamentals. *Innovative Food Science & Emerging Technologies*, 2013; 19: 1–14.
- [13] Barbin D F, ElMasry G, Sun D W, Allen P. Non-destructive determination of chemical composition in intact and minced pork using near-infrared hyperspectral imaging. *Food Chemistry*, 2013; 138(2): 1162–1171.
- [14] Bhuvaneswari K, Fields P G, White N D, Sarkar A K, Singh C B, Jayas D S. Image analysis for detecting insect fragments in semolina. *Journal of Stored Products Research*, 2011; 47(1): 20–24.
- [15] Serranti S, Cesare D, Marini F, Bonifazi G. Classification of oat and groat kernels using NIR hyperspectral imaging. *Talanta*, 2013; 103: 276–284.
- [16] Choudhary R, Mahesh S, Paliwal J, Jayas D S. Identification of wheat classes using wavelet features from near infrared hyperspectral images of bulk samples. *Biosystems Engineering*, 2009; 102(2): 115–127.
- [17] Fawcett J K. The semi-micro Kjeldahl method for the determination of nitrogen. *The Journal of Medical Laboratory Technology*, 1954; 12(1): 1–22.
- [18] Chang S K. *Protein analysis. Food analysis*. Springer, US, 2010. Chapter 9, pp.133–146.